Shape and Surface Roughness Effects on Turbulent Nosetip Ablation

W. E. Welsh Jr.*
The Aerospace Corporation, El Segundo, Calif.

A simplified analysis is performed for first-order estimates of shape and surface roughness effects on turbulent ablation of a re-entry body nose surface. The analysis treats the stable turbulent ablated nose shape formed on an ablating cylinder in parallel hypersonic flow. It is assumed that: turbulent boundary-layer flow exists over the entire nose, a stable shape solution exists, surface pressures are Newtonian, and boundary-layer edge properties are given by isentropic expansion of flow that entered the shock layer through a normal shock. A flat-plate reference enthalpy relation is used to describe turbulent heating. In addition, an approximate analysis is presented for the effect of ablative material surface roughness on the recession rate of the turbulent shape. It is found that for the cases of $\gamma = 1.2$, 1.4, and 1.585, a power-law nose shape is predicted with $r \propto z^{0.75}$, except near the axis of symmetry where $r \propto z^{0.80}$ and the sonic point is located at about two-thirds of the body radius aft of the forward tip. Also, it is found that ablative material surface roughness of 0.001 in. can cause significant increases in recession rate at stagnation point pressures over 10 atm for representative re-entry conditions and body sizes. The applicability of these results for the evaluation of re-entry body shape change and recession rate is discussed.

Nomenclature

c_p = specific heat
h = enthalpy including dissociation energy
K_r = heat flux ratio, q_w/q_w (smooth surface)
k = roughness height (or thermal conductivity)
Nu = Nusselt number, $q_w c_p x[k(h_e - h_w)]$
Q^* = heat of ablation, $q_w/(\rho_s \dot{s})$
q_w = heat flux to body surface
P = pressure
Pr = Prandtl number
R = radius of curvature
r = radial coordinate
Re_d = diameter Reynolds number, $\rho u d/\mu$
Re_x = length Reynolds number, $\rho_e u_e x/\mu_e$
Re_k = roughness Reynolds number, $\rho_k u_k k/\mu_k$
Re_θ = momentum thickness Reynolds number, $\rho_e u_e \theta/\mu_e$
$\dot{s}$ = recession rate
u = streamwise velocity
x = distance along surface
z = axial coordinate
α = surface angle
θ = momentum thickness
ρ = density

Superscripts and subscripts

$( )'$ = reference condition
a = axial direction
b = body
d = diameter
e = edge of boundary layer
k = evaluated at roughness height
s = solid
w = wall
x = length
θ = evaluated using momentum thickness
$*$ = sonic point condition
∞ = freestream condition
0 = stagnation point value
1,2 = limits of roughness regime; see Eqs. (10–12)

Received June 12, 1969; presented as Paper 69-717 at the AIAA Fluid and Plasma Dynamics Conference, San Francisco, Calif., June 16–18, 1969; revision received March 9, 1970. The author is indebted to H. Mirels of The Aerospace Corporation for his assistance and encouragement in this study. This research was supported by the U. S. Air Force under Contract No. F04701-68-C-0200.

* Member of the Technical Staff, Aerodynamics and Propulsion Research Laboratory; presently Staff Engineer, San Bernardino Operations, The Aerospace Corporation, San Bernardino, Calif.

I. Introduction

Although considerable attention has been given to laminar ablation of the nose region of re-entry bodies, relatively little information is available for the case of turbulent boundary-layer flow over the nose. On the basis of results of transition experiments on hemispheres,[1,2] it can be expected that, at sufficiently high Reynolds numbers, turbulent boundary-layer flow will exist starting from a location close to the stagnation point on an ablating nose. Consider the nose region between the stagnation point and the sonic point on a body in hypersonic flow. It is of interest to determine the stable ablated nose shape† and recession rate for the turbulent flow case. The influence of surface roughness of the ablating material under these conditions is also of potential significance. The present work treats the nose region ablation of a cylinder in parallel, hypersonic flow in order to provide first-order estimates of these effects on re-entry bodies.

Experimental studies[3,4] have indicated that, under low Reynolds number conditions where the nose region boundary layer is laminar, an initially hemispherical ablating body will evolve into a somewhat blunter shape. However, for higher Reynolds number conditions, several investigators[4,5] have reported development of an ogival-shaped nose that is clearly distinguishable from the laminar shape. Examples of the two characteristic ablated nose shapes are shown in Fig. 1, from the work of Miller and Sutton.[4] Shape B in Fig. 1 is a typical laminar ablated shape. The ogival shape (C) is assumed to be caused by turbulent boundary-layer flow over the nose on the basis of qualitative similarity to the theoretical results of Murzinov[6] for transient shape change of initially hemispherical nose surfaces. Murzinov's analysis did not extend to large times, where a time-independent, stable shape may exist. Further, his work utilized a turbulent heating distribution that did not adequately account for streamwise length dependence of heating. No analysis is presently

† It is assumed that, regardless of the initial shape, the nose will approach a stable shape after a sufficient time period.

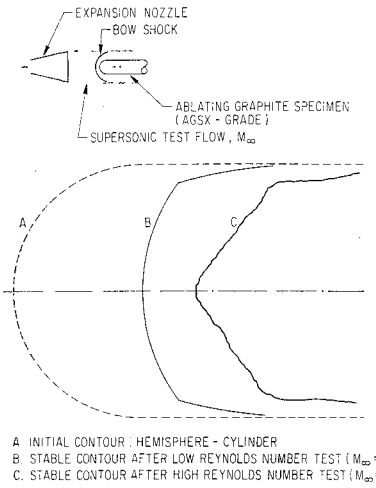

Fig. 1 Ablated nose shape results of Miller and Sutton.

available of the stable turbulent ablated nose shape. Analyses are available, however, for stable laminar ablated shapes.[3,7]

The present work follows the general method of stable shape analysis used in previous laminar shape analyses such as those of Benjamin[7] and Simpkins,[3] in which general relations for pressure and heat-transfer distributions are postulated and the resulting shape is solved for from a set of simultaneous algebraic equations. Complexities of non-Newtonian surface pressures and variable-entropy boundary-layer edge conditions are avoided by restriction of the analysis to the subsonic flow region on the nose. The flat-plate reference-enthalpy relation is used for a general turbulent heat-transfer distribution. An estimate of the increased heat transfer due to surface roughness, based on correlations of experimental results in tube flow, is presented. After determination of the stable turbulent shape and roughness effects on heating, a simple method of calculating the axial recession rate is given that uses the sonic point heating rate. Typical results for the effect of surface roughness on the stable turbulent ablated contour recession rate are illustrated for a range of body sizes, roughness heights, and pressures. Applicability of these results to re-entry body flight and ground tests is discussed.

II. Stable Turbulent Ablated Nose Shape

A brief analysis will be performed to obtain a description of the turbulent subsonic flow region on an ablating nosetip. This is a significant region for roughness effects (to be treated later) since the local Reynolds number is high and consequently yields thin boundary layers that are susceptible to surface disturbances. The analysis is performed to find the stable geometrical contour of the nose surface on an ablating cylinder in parallel hypersonic flow. The geometry to be analyzed and the coordinates are shown in Fig. 2. The primary assumptions for the analysis are as follows: 1) the shape is time-independent, or stable, in nose-fixed coordinates; 2) the oncoming flow is steady and uniform; 3) transition occurs at an infinitesimal distance from the axis, yielding turbulent boundary layer flow over the nose surface; 4) the turbulent heating distribution can be expressed by the flat plate reference enthalpy (FPRE) relation; 5) surface pressure can be expressed by a modified Newtonian relation; 6) boundary-layer edge conditions for the entire nose region can be approximated by isentropic expansion of flow from the stagnation point pressure to the local surface pressure; 7) the local recession rate of ablative material is linearly related to the local hot-wall nonblowing heating rate q_w through the heat of ablation Q^*, and Q^* is taken to be constant; 8) surface temperature is uniform and constant; and 9) the sonic point is located at the cylinder radius, and no ablation occurs on the cylindrical surface of the body.

Assumption 9 requires that the body radius remain constant downstream of the sonic point. The analysis is thus performed for the surface between the axis and the sonic point, which is denoted as the nose region. In this region, geometry requires that the normal and axial recession components be related by

$$\dot{s}_a = \dot{s}/\sin\alpha = \text{const} \tag{1}$$

for stable profile shape. Thus, surfaces at smaller angles α have smaller local normal recession rates $\dot{s}$. The surface angle α_* at the sonic point is considered given for specified gas properties. The problem, then, is to find the variation of surface angle α for $0 < r < r_*$ and $\alpha_0 > \alpha > \alpha_*$. The surface angle α_0 at $r = 0$ may or may not be $\pi/2$.

From Assumption 7 and Eq. (1) the heating rate distribution becomes

$$q_w(r)/q_w(r_*) = \dot{s}(r)/\dot{s}(r_*) = \sin\alpha/\sin\alpha_* \tag{2}$$

The flat plate reference enthalpy (FPRE) relation‡ can be expressed, with the use of $(\ )'$ to denote the reference state for variable properties, as

$$Nu_x' = 0.030 Pr'^{1/3}(Re_x')^{0.8} \tag{3}$$

With Assumptions 4 and 8, Eq. (3) yields the following heating rate distribution, neglecting viscosity variations:

$$q_w(r)/q_w(r_*) = [(\rho_e u_e)/(\rho_e u_e)_*]^{0.8}[x(r)/x(r_*)]^{-0.2} \tag{4}$$

Equations (2) and (4) are combined to yield

$$[(\rho_e u_e)/(\rho_e u_e)_*]^{0.8}[x(r)/x(r_*)]^{-0.2} = \sin\alpha/\sin\alpha_* \tag{5a}$$

or

$$x(r)/x(r_*) = (\sin\alpha/\sin\alpha_*)^{-5}[(\rho_e u_e)/(\rho_e u_e)_*]^4 \tag{5b}$$

The surface pressure in hypersonic flight with a thin shock layer parallel to the local body surface is given by the modified Newtonian relation

$$P/P_0 = \sin^2\alpha \tag{6}$$

For a given specific heat ratio γ the local mass flux ratio $(\rho_e u_e)/(\rho_e u_e)_*$ can be expressed as a function of α from Assumption 6, Eq. (6), and isentropic flow relations. The nondimensional surface length from Eq. (5b) can then be expressed as

$$x(r)/x(r_*) = f_1(\gamma,\alpha) \tag{7}$$

To obtain the equation for the nose shape in cylindrical coordinates r and z, we note that $dr = dx\sin\alpha$ and $dz = dx\cos\alpha$.

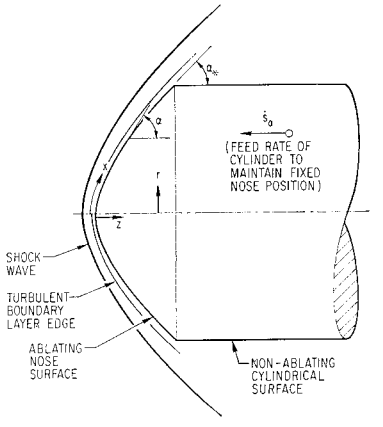

Fig. 2 Geometry for turbulent shape analysis.

‡ Cresci, MacKenzie, and Libby[8] found that this relation adequately predicted turbulent heat transfer to an experimental hemisphere-cone body. It is also approximately correct for sharp cones and, hence, should give reasonable results for more general shapes.

Thus the coordinates can be expressed as

$$\frac{r}{r_b} = \left(\int_{\alpha_0}^{\alpha} \frac{df_1}{d_\alpha} \sin\alpha d\alpha\right) \Big/ \left(\int_{\alpha_0}^{\alpha_*} \frac{df_1}{d_\alpha} \sin\alpha d\alpha\right) \quad (8a)$$

$$\frac{z}{r_b} = \left(\int_{\alpha_0}^{\alpha} \frac{df_1}{d_\alpha} \cos\alpha d\alpha\right) \Big/ \left(\int_{\alpha_0}^{\alpha_*} \frac{df_1}{d_\alpha} \sin\alpha d\alpha\right) \quad (8b)$$

Because of the character of the integrals for r and z, it is not possible to formulate an exact expression for r as an explicit function of z. Solutions obtained for specific heat ratios of interest are discussed in Sec. V. A discussion of integration methods used in obtaining these solutions is presented in the Appendix.

III. Surface Roughness Effects

Previous studies of boundary-layer flow over rough nonablating surfaces have shown that roughness can cause premature boundary-layer transition,[2] increased wall shear,[9] and increased convective heating.[10] Most ablation materials of interest have a granular microstructure, which may cause some inherent surface roughness. Relations are derived in this section to estimate the effect of such surface roughness on the heating rate to the stable turbulent ablating nose shape.

The assumptions for this analysis are as follows.

1) There exists an asymptotic limit to the ratio of fully-rough-to-smooth wall heat transfer to a flat plate in turbulent flow, and the value of that limit, as found by Dippree and Sabersky[10] for fully developed incompressible turbulent tube flow at Prandtl numbers near unity, is approximately 3.

2) The Reynolds number regime Re_{x_1} to Re_{x_2} (for a given roughness height-to-length ratio k/x) where a transition occurs between smooth and rough wall heat transfer in turbulent flat plate flow is identical to that predicted by Schlichting[9] for shear on a rough flat plate (Re_x is evaluated with reference enthalpy properties to account for large property variations).

3) The normalized variation of heat transfer with Reynolds number in the transitional regime between smooth and fully-rough wall conditions on a flat plate is similar to that found[10] for tube flow by substituting Re_x for Re_d.

4) The effect of roughness on turbulent heating in a pressure gradient can be treated like that on a flat plate at the local Reynolds number Re_x and streamwise length x.

5) Roughness height k (i.e., effective sand roughness) is given and constant.

6) All assumptions in Sec. II for the stable shape hold.

We denote the ratio of heating rate with roughness to that for a smooth surface as K_r. Note that from Assumption 1,

$$1 < K_r < 3 \quad (9)$$

Dippree and Sabersky[10] have measured wall heat transfer with incompressible turbulent flow in a rough tube and found the heating rate to be a function of Re_d and k/d. A simple correlation of their result is

$$K_r \cong 1 + 2[(Re_d - Re_{d_1})/(Re_{d_2} - Re_{d_1})], \quad Re_{d_1} < Re_d < Re_{d_2} \quad (10a)$$

$$K_r = 1, \; Re_d < Re_{d_1} \quad (10b)$$

$$K_r \cong 3, \; Re_d > Re_{d_2} \quad (10c)$$

(Note that Re_{d_1} and Re_{d_2} are functions of k/d that need not be specified here.) From Assumptions 1 and 3 we can find K_r for a rough flat plate by replacing $(\;)_d$ in Eqs. (10) with $(\;)_x'$. Schlichting[9] shows wall shear estimates for incompressible turbulent flow over a rough flat plate, from which the limits Re_{x_1} and Re_{x_2} (of the Reynolds number regime over which wall shear undergoes a transition from smooth to fully rough limits) can be correlated as

$$Re_{x_1} \cong 47(k/x)^{-1.081} \quad (11a)$$

$$Re_{x_2} \cong 670(k/x)^{-1.081} \quad (11b)$$

With Assumption 2, Re_{x_1}' and Re_{x_2}' values for K_r on a flat plate can be evaluated from the right-hand sides of Eqs. (11a) and (11b), respectively. Thus, we obtain for K_r on a flat plate, from Eqs. (10) (with Re_x' substituted for Re_d) and Eqs. (11a) and (11b)

$$K_r \cong 1 + (2/13.25)(\{Re_x'/[47(x/k)^{1.081}]\} - 1), \quad Re_{x_1}' < Re_x' < Re_{x_2}' \quad (12a)$$

$$K_r = 1, \; Re_x' < Re_{x_1}' \quad (12b)$$

$$K_r \cong 3, \; Re_x' > 14.25 Re_{x_1}' \quad (12c)$$

This result for K_r is used in the calculation of heat transfer and recession rate in Sec. IV.

Since K_r indicates the ratio of local wall heating in a pressure gradient to the smooth wall heating (from Assumption 4) given by Eq. (3), it follows that the heat-transfer rate ratio of Eq. (4) requires modification to account for any variation of K_r along the surface for the case of surface roughness. Thus, the shape result of Sec. II [see Eqs. (8)] would be altered if K_r varies along the surface. Such modified shapes are not derived here, however. According to the assumptions of this analysis, the axial recession rate of the stable contour can be determined by calculation of sonic point phenomena, and thus the altered shape with roughness should not change the recession rate result to be shown next.

IV. Axial Recession Rate

On the basis of the foregoing assumptions and analysis, a relation for the axial recession rate $\dot{s}_a$ of the stable turbulent ablating contour that includes surface roughness effects can be derived. It is convenient to calculate this rate using sonic point conditions because the significant parameters $\rho_e u_e$ and α are most easily obtained at that point on the contour. The local normal recession rate, from the defining relation for heat of ablation Q^*, is

$$\dot{s} = q_w/(\rho_s Q^*) \quad (13)$$

where ρ_s is the density of the solid phase of ablating material, and other terms are as previously defined. From Eqs. (1) and (13) the axial recession rate is

$$\dot{s}_a = \dot{s}/\sin\alpha = (\dot{s})_*/\sin\alpha_* = (q_w)_*/(\rho_s Q^* \sin\alpha_*) \quad (14)$$

From Assumptions 4, 7, and 8 in Sec. II, Eqs. (5) and (12), and the definition of Nusselt number Nu_x', $(q_w)_*$ can be calculated for given flow conditions, cylinder radius r_b, and surface roughness k. The product $\rho_s Q^*$ can be specified for a given ablation material. The value of $\sin\alpha_*$ can be obtained, from relations in Sec. II, for a given specific heat ratio γ.

V. Results

Stable turbulent ablated nose shape results have been obtained from Eqs. (8a) and (8b) for several gas specific heat ratios of interest; these results were obtained with integration methods shown in the Appendix. The specific heat ratios and corresponding sonic point surface angles studied were $\gamma = 1.2$, $\alpha_* = 48.767°$; $\gamma = 1.4$, $\alpha_* = 46.633°$; $\gamma = 1.585$, $\alpha_* = 45.0°$. The results of these calculations are shown in Figs. 3a and 3b. The logarithmic plot in Fig. 3a indicates similar exponential behavior for the three cases. It was found that the results approximated $r \propto z^{0.8}$ for $r \ll r_b$ and $r \propto z^{0.75}$ for $r \sim r_b$. The linear plot in Fig. 3b indicates the visual appearance of the stable shapes. The major difference found is the small extension of axial length caused by larger γ. If this effect were eliminated by appropriate replotting, the nondimensional shape results would be negligibly different for the three cases studied. An approximate formula for nose

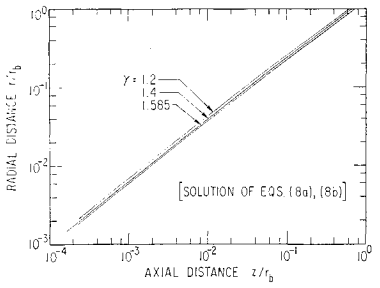

Fig. 3a Logarithmic plot of stable turbulent shape.

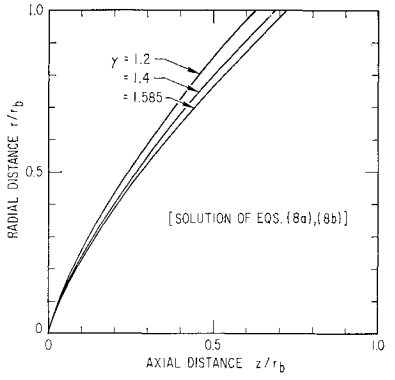

Fig. 3b Linear plot of stable turbulent shape.

shape for the case of $\gamma = 1.2$ (applicable for high-temperature air conditions) is

$$(r/r_b) = 1.422(z/r_b)^{0.75},\ 0.01 < r/r_b \leq 1.0 \qquad (15)$$

except for locations very near the axis, where the exponent is 0.8.

Because the shape result for hypersonic flight is somewhat similar to a sharp cone of half-angle α_*, one can obtain a qualitative estimate of the effect of lower flight Mach numbers on the gross shape by referring to inviscid flow results[11] for sharp cones. Figure 4 shows the required cone half-anlge for sonic flow at the cone surface as a function of flight Mach number. Thus it can be estimated that a sharper nose shape will result for turbulent flow at Mach numbers less than 6 if sonic flow is to be maintained at the outer edge.

Figure 5 shows the regimes of stagnation pressure and surface roughness where roughness can affect the sonic point turbulent heating rate for a specified flight condition and surface temperature. These results are obtained from Eq. (12) for K_r with the use of standard approximations for properties of air. The flight velocity of 17,350 fps and surface temperature of 4000°K were arbitrarily selected. Three values of cylinder radius r_b are indicated. As can be deduced from Eq. (12a), r_b has only a slight effect on K_r.

Also shown in Fig. 5 are estimated conditions for normal (smooth-wall) and premature (roughness-induced) transition at the sonic point of a stable laminar ablated nose. This shape was taken to be a spherical segment of radius $R = (2)^{1/2}r_b$ on the basis of the experimental results of Miller and Sutton[4] for ablating cylinders. Normal transition was assumed to occur at a momentum thickness Reynolds number Re_θ of 250 on the basis of the results of Stetson.[1] Roughness-induced transition was assumed to occur at a roughness Reynolds number Re_k of 130 on the basis of the results of Bandettini and Isler[2] for transition on roughened hemispheres and on the effect of wall cooling postulated by Dunlap and Kuethe.[12] These transition estimates indicate that, when roughness-induced transition occurs, the resulting turbulent boundary layer is immediately disturbed by surface roughness.

The effect of surface roughness on recession rate of the stable turbulent ablated contour, from Eq. (14), is shown in Figs. 6a, 6b, and 6c for the example reentry condition of Fig. 5 and for three body sizes. The recession rate is made dimensionless with an arbitrary reference value that is common to the three figures; thus the results are not restricted to a particular ablative material or Q^* value. Laminar stable contour recession rates (based on laminar stagnation point heating[13]) for a spherical segment of $R = (2)^{1/2}r_b$ are shown for comparison. A Lewis number of unity and fully recombined species at the wall were assumed for both laminar and turbulent heat transfer calculations.§

VI. Discussion

The analysis and results presented here relate to an idealized model formulated mainly for simple estimates of the turbulent boundary-layer effect on a stable nose shape and of surface roughness effects on the axial recession rate of that shape. Accordingly, it is anticipated that the results will be of most value in illustrating qualitative features of these effects under experimental conditions with specific ablation materials. Some of the major assumptions and possible inaccuracies are discussed with regard to engineering applications.

It has not been established analytically that an asymptotic limit exists for the ablated shape of a given ablating configuration. However, the experimental results of Miller and Sutton[4] and Simpkins[3] suggest that such a limit is approached for long durations of ablation. Murzinov's analytical results[6] for transient laminar and turbulent ablation also suggest that shape similarity is approached for large times. If such a limit exists, it is apparent that a characteristic time of the order of $r_b/\dot{s}_a$ would be required to develop a new nose shape. It should be noted that Benjamin,[7] Simpkins,[3] and Sutton[14] have previously assumed the existence of stable or quasi-steady states in the analysis of laminar ablated shapes. Two factors in re-entry ablation problems could interfere with the formation of a stable nose shape. First, the oncoming flow conditions could be strongly time-dependent. Second, the scale of the nose can be influenced by transient ablation of downstream surfaces, even for constant oncoming flow conditions. This would be more significant for conical afterbodies with large cone angles.

The scale of the nose region (as defined here) for a cylinder in parallel flow is probably different, even for a stable shape situation, from that assumed here. Obviously, ablation can indeed occur on surfaces with locally supersonic flow at the boundary-layer edge. The calculation of stable shape for that case will be more complex than the present analysis because of the need to determine local (non-Newtonian) surface

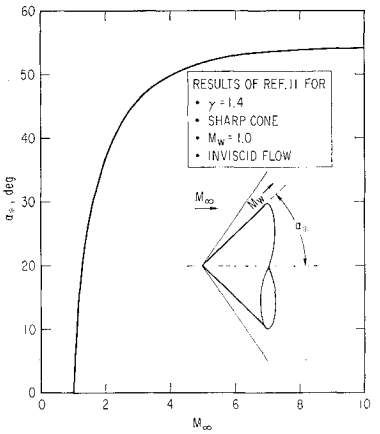

Fig. 4 Effect of flight Mach number on surface angle for sonic flow at a cone surface.

§ Figures 6a, 6b, and 6c can also be interpreted in terms of hot wall heating rate vs pressure by use of a linear scale conversion with a heating rate of 1000 Btu/ft² sec located at unity $\dot{s}/\dot{s}$ (ref). (Note the $\sin\alpha_*$ factor between turbulent heating and axial recession rate.)

pressures and $\rho_e u_e$ for variable entropy conditions. It can be noted, however, that even for scale reduction of the sonic point radius to values like $r_b/10$, the recession rate for turbulent boundary-layer flow will increase only by 59%, because $\dot{s}_a \propto (q_w)_* \propto x_*^{-0.2} \simeq r_b^{-0.2}$. With surface roughness, however, such a scale change could cause considerably larger nose recession because of the larger value of k/x achieved, with a consequent increase in K_r and q_w.

It can be shown that the local $\rho_e u_e$ product as obtained from Assumption 6 in Sec. II is inaccurate for shapes approaching sharp cones (such as those in Fig. 3). Near the outer radius at α_*, the $\rho_e u_e$ value is probably closer to that given by cone flow relations. An estimate has been made of the difference between the isentropic expansion result and cone flow result for $(\rho_e u_e)_*$ with $\gamma = 1.4$. The ratio of cone flow $\rho_e u_e$ to isentropic $\rho_e u_e$ at α_* was 1.495; the axial recession rate (evaluated with the use of sonic point $\rho_e u_e$) was 38% higher with cone values. No evaluation was made of the corresponding change of stable nose shape. The new shape corrected for variable entropy effects would be slightly sharper near the axis [from Eq. (7)]. Future analyses could use more elaborate shock layer relations to improve on the present work.

Direct application of the asymptotic limiting ratio of fully-rough-to-smooth surface heat transfer found in tubes to the case of flat plate and pressure-gradient flows, as made in Assumptions 1 and 4 in Sec. III, is justified solely on the basis of simplicity at present. Experimental data are required to establish the validity of these assumptions.

If boundary-layer transition on the nose surface occurs at some appreciable distance from the axis, then a stable shape could develop that corresponds to laminar boundary-layer flow in a central region and turbulent flow over the outer region. Experiments are required to establish the conditions under which the entire nose surface boundary layer is turbulent, as assumed in this analysis.

A primary question for engineering purposes concerns the magnitude of surface roughness for estimates of boundary-layer transition and increased turbulent heating and nose recession rates. The effective surface roughness presumably depends on the ablation material considered, its microstructure, the mode of ablation, and boundary-layer flow conditions. The present results, although providing no data on roughness for specific materials, indicate that only small values of effective surface roughness are required for significant effects on nose recession rate. Accurate determination of in-process surface roughness may, in fact, be difficult to accomplish in a direct manner. However, it may be possible to estimate roughness by comparison of experimental recession rate results with analytical predictions such as those presented here.

More accurate recession rate analyses can be performed for specific ablation materials with the use of relations accounting for the variability of the effective heat of ablation Q^* with boundary-layer conditions. A constant Q^* was assumed herein only for purposes of illustration of other effects on shape and recession rate. An important component of Q^* is the blowing effectiveness, which describes the reduction of convective heating as a function of the mass injection rate. It is probable that the blowing effectiveness will decrease as surface roughness begins to disturb the boundary layer; detailed recession rate predictions will depend upon determination of the extent of the decrease. It is evident that greater differences than those shown here between laminar and rough-turbulent recession rates will be predicted if the lower Q^* under turbulent conditions, and even lower Q^* with a degraded blowing effectiveness due to roughness, are used.

Ground tests of ablating bodies under conditions where turbulent boundary layers and roughness effects can exist on

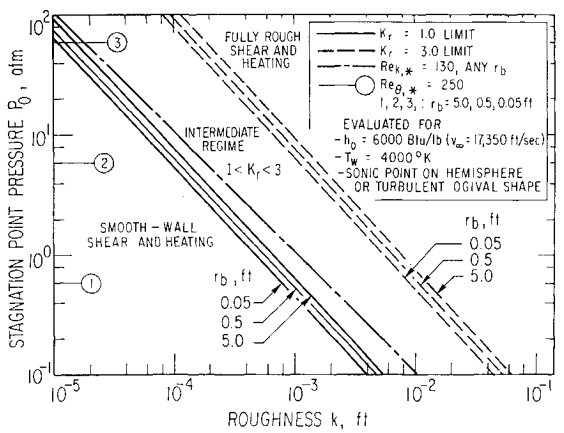

Fig. 5 Regimes of surface roughness effects.

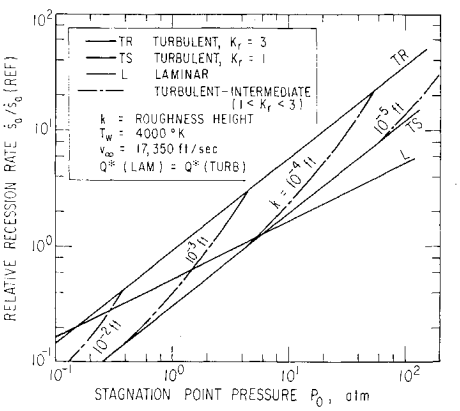

Fig. 6a Nose surface recession for r_b = 0.05 ft.

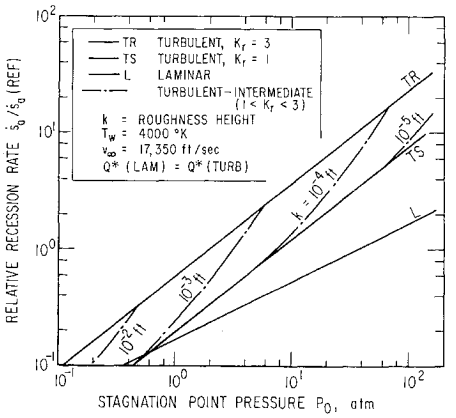

Fig. 6b Nose surface recession for r_b = 0.5 ft.

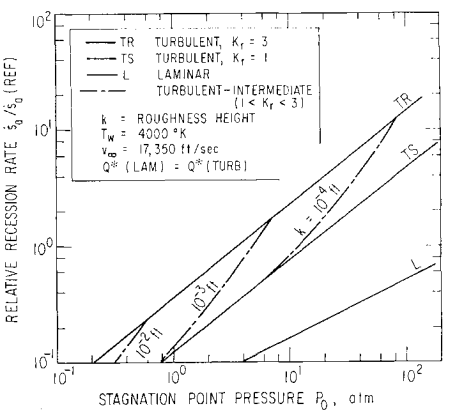

Fig. 6c Nose surface recession for r_b = 5.0 ft.

the nose require evaluation of simulation parameters for these effects in addition to parameters typically considered. The present results suggest that test results will be sensitive to the average flow Mach number, Mach number gradients, stream turbulence level, body scale, and sonic point Reynolds number. Further, the sensitivity of test results to these parameters will be different for the laminar and turbulent cases.

VII. Conclusions

An analysis has been presented of the stable ablating nose shape and nose recession rate under turbulent boundary-layer conditions. This analysis is based on a set of simplifying assumptions for a cylinder in parallel hypersonic flow. An estimate has been made of the effect of surface roughness on the nose recession rate.

Stable turbulent ablated nose shapes were predicted for gas specific heat ratios of $\gamma = 1.2$, 1.4, and 1.585. These shapes were found to approximate power law shapes where $r \propto z^{0.8}$ at $r \ll r_b$ and $r \propto z^{0.75}$ at $r \sim r_b$. The axial position of the sonic point was found to be between $0.625\, r_b$ and $0.722\, r_b$. The dependence of nose shape on flight Mach number was noted.

Surface roughness, characteristic of some ablating materials, was found to cause significant increases in nose recession rate, even for roughness heights as small as 1×10^{-3} in., at re-entry stagnation-point pressure levels above 10 atm and over a range of body radius from 0.05 to 5 ft.

The present results are qualitatively indicative of nose shape and surface roughness effects on slender ablative reentry vehicle nosetips. Anticipated differences between the present results and results from experimental situations have been noted. The main conclusion that can be made at present is that, where turbulent boundary-layer flow occurs on the nose of an ablating body, both flight and ground test results can be significantly influenced by the effects of shape development and surface roughness. More extensive analyses are required to establish the nature and extent of these effects for specific geometries, materials, and environmental conditions.

Appendix: Integration Methods for Eqs. (8a) and (8b)

A. Special Case of $\gamma = 1.585$

In the case of $\gamma = 1.585$, it can be shown that $\alpha_* = \pi/4$ from Eq. (6), Assumption 6 in Sec. II, and isentropic flow relations. It can also be shown that, within an accuracy of several percent, the mass flux ratio for this case can be approximated by

$$(\rho_e u_e)/(\rho_e u_e)_* = \sin(2\alpha) \tag{A1}$$

Thus the expression f_1 in Eq. (7) becomes

$$f_1(\alpha) = 2^{-5/2}(\sin\alpha)^{-5}(\sin 2\alpha)^4 \tag{A2}$$

The derivative $df_1/d\alpha$ is easily obtained for this case for use in Eqs. (8a) and (8b). Both equations can be integrated exactly in this case. Inspection of Eq. (A2) shows that α_0 must be $\pi/2$ in order for f_1 (i.e., x/x_*) to vanish at the axis, and the result of integration is

$$r/r_b = (1/a_1)[(\tfrac{3}{4})\cos^4\alpha - (\tfrac{1}{2})\cos^2\alpha - \log_e(\sin\alpha)] \tag{A3a}$$

$$z/r_b = (1/a_1)[(\tfrac{3}{8})\alpha + (\tfrac{1}{4})\sin 2\alpha + (\tfrac{1}{32})\sin 4\alpha + (\cos^7\alpha)/(\sin\alpha) + \cos^5\alpha\sin\alpha - (\tfrac{3}{16})\pi] \tag{A3b}$$

where

$$a_1 \equiv [(\tfrac{3}{4})\cos^4(\pi/4) - (\tfrac{1}{2})\cos^2(\pi/4) - \log_e(\sin\pi/4)] = 0.284$$

These expressions are evaluated over a range of $\pi/2 > \alpha > \pi/4$, permitting tabular or graphical presentation of r/r_b and z/r_b at common values of α.

B. General Case of Arbitrary γ

From standard isentropic flow relations for M and $(\rho u)/(\rho u)_*$ [i.e., $1/(A/A_*)$] and the modified Newtonian surface pressure relation [Eq. (6)], the following expression for mass flux can be derived

$$(\rho_e u_e)/(\rho_e u_e)_* = [(2)/(\gamma - 1)]^{1/2}\cdot[(\gamma + 1)/2]^{(\gamma+1)/[2(\gamma-1)]} \times (\sin\alpha)^{(\gamma+1)/\gamma}\cdot[(\sin\alpha)^{[2(\gamma-1)]/\gamma} - 1]^{1/2} \tag{A4}$$

Thus f_1 in Eq. (7) becomes

$$f_1(\alpha) = (\sin^5\alpha_*)/(\sin^5\alpha)a_2^4(\sin\alpha)^{[4(\gamma+1)]/\gamma}[(\sin\alpha)^{[2(\gamma-1)]/\gamma} - 1]^2 \tag{A5}$$

where

$$a_2 \equiv [2/(\gamma - 1)]^{1/2}[(\gamma + 1)/2]^{(\gamma+1)/[2(\gamma-1)]}$$

The derivative $df_1/d\alpha$ is then obtained and inserted into the integral expressions for r and z. It is found that the expression for r [Eq. (8a)] can be integrated exactly for arbitrary γ. Inspection of Eq. (A5) shows that α_0 must be $\pi/2$ in order for f_1 (i.e., x/x_*) to vanish at the axis. The expression for radius is found to be

$$r/b = [(2n + m)/(m + 2n + 1)][(\sin\alpha)^{m+2n+1} - 1] - [(2n + 2m)/(m + n + 1)][(\sin\alpha)^{m+n+1} - 1] + [m/(m + 1)][(\sin\alpha)^{m+1} - 1] \tag{A6}$$

where $b \equiv x_* a_2^4 \sin^5\alpha_*$, $m \equiv (4 - \gamma)/\gamma$, $n \equiv 2(1 - \gamma)/\gamma$. The expression for z [Eq. (8b)] cannot be integrated exactly. The following integral expression for z was evaluated by numerical methods:

$$\frac{z}{b} = (2n + m)\int_{\pi/2}^{\alpha}(\cos\alpha)^2(\sin\alpha)^{m+2n-1}d\alpha - (2n + 2m)\int_{\pi/2}^{\alpha}(\cos\alpha)^2(\sin\alpha)^{m+n-1}d\alpha + (m)\int_{\pi/2}^{\alpha}(\cos\alpha)^2(\sin\alpha)^{m-1}d\alpha \tag{A7}$$

where b, m, and n are defined as for Eq. (A6).

Expressions (A6) and (A7) for r and z, respectively, were evaluated over a range of $\pi/2 > \alpha > \alpha_*$ to permit tabular or graphical presentation of r/r_b and z/r_b at common values of α. Here the reference parameter r_b is simply $r(\alpha_*)$ from Eq. (A6). Thus, the parameter b is eliminated in the presentation of r/r_b and z/r_b.

References

[1] Stetson, K. G., "Boundary Layer Transition on Blunt Bodies with Highly Cooled Boundary Layers," *Journal of the Aerospace Sciences*, Vol. 27, No. 2, Feb. 1960, pp. 81–91.

[2] Bandettini, A. and Isler, W. S., "Boundary Layer Transition Measurements on Hemispheres of Various Surface Roughness in a Wind Tunnel at Mach Numbers from 2.48 to 3.55," Memo 12-25-58A, March 1959, NASA.

[3] Simpkins, P. G., "On the Stable Shape of Subliming Bodies in a High-Enthalpy Gas," *Journal of Fluid Mechanics*, Vol. 15, No. 1, Jan. 1963, pp. 119–132.

[4] Miller, I. M. and Sutton, K., "An Experimental Study of the Oxidation of Graphite in High Temperature Supersonic and Hypersonic Environments," TN D-3444, July 1966, NASA.

[5] Palkin, S. N. et al., "Investigation of the Ablation of Low-Melting Models in a Ballistic Facility," *Aerofizicheskiye Issledovaniya Sverkhzvukovykh-Technii*, Nauka Press, Moscow, 1967, pp. 274–283; English translation TT F-11, 309, Nov. 1967, NASA.

[6] Murzinov, I. N., "Concerning the Shape of Bodies Ablating Under the Action of Intense Heating During a Motion in the

Atmosphere," *Izvestiya Akademii Nauk SSSR, Otdelenie Tekhnicheskikh Nauk, Mekhanika i Mashinostroenie*, No. 4, 1965, pp. 36–40.

[7] Benjamin, A. S., "The Effect of Albative Geometry Change on the Heating and Recession Characteristics of Sphere-Cones," AIAA Paper 66-992, Boston, Mass., 1966.

[8] Cresci, R. J., MacKenzie, D. A., and Libby, P. A., "An Investigation of Laminar, Transitional, and Turbulent Heat Transfer on Blunt-Nosed Bodies in Hypersonic Flow," *Journal of the Aerospace Sciences*, Vol. 27, No. 6, June 1960, pp. 401–414.

[9] Schlichting, H., *Boundary Layer Theory*, McGraw-Hill, New York, 1955, pp. 447–449.

[10] Dippree, D. F. and Sabersky, R. H., "Heat and Momentum Transfer in Smooth and Rough Tubes at Various Prandtl Numbers," *International Journal of Heat and Mass Transfer*, Vol. 6, No. 5, May 1963, pp. 329–353.

[11] Ames Research Staff, "Equations, Tables, and Charts for Compressible Flow," Rept. 1135, 1953, NACA.

[12] Dunlap, R. and Kuethe, A. M., "Effects of Cooling on Boundary Layer Transition on a Hemisphere in Simulated Hypersonic Flow," *Journal of the Aerospace Sciences*, Vol. 29, No. 12, Dec. 1962, pp. 1454–1461.

[13] Fay, J. A. and Riddell, F. R., "Theory of Stagnation Point Heat Transfer in Dissociated Air," *Journal of the Aerospace Sciences*, Vol. 25, No. 2, Feb. 1958, pp. 73–85.

[14] Sutton, G. W., "On the Stable Shape of a Slender Ablating Graphite Body," *Journal of the Aerospace Sciences*, Vol. 26, No. 10, Oct. 1959, pp. 681–682.

NOVEMBER 1970 AIAA JOURNAL VOL. 8, NO. 11

Thermal Degradation Kinetics and Surface Pyrolysis of Vinyl Polymers

G. LENGELLE*
University of California, San Diego, La Jolla, Calif.

Explicit expressions are obtained for the surface regression rates of pyrolyzing vinyl polymers. Thermal degradation of the polymer in a subsurface reaction zone is assumed rate limiting. Emphasis is placed on determination of the proper degradation mechanism (e.g., mode of initiation and magnitude of the kinetic chain length compared to the degree of polymerization), development of kinetic data, and derivation of corresponding expressions for the rate of mass loss. The method of calculation is based on a matched asymptotic expansion scheme, with the nondimensional activation energy, $\varepsilon = E/R^0T_s \gg 1$, treated as the expansion parameter. Results are displayed for polytetrafluoroethylene and compared to experimental results with fair success for polymethylmethacrylate and polystyrene.

Nomenclature

A = $[\Delta H_s(q_0 + N_w)]^{1/2\delta} \exp[\varepsilon_w(1 - \gamma)]$
B = pre-exponential factor in rate constants, sec^{-1}
c = specific heat at constant pressure
d = thermal diffusivity deep within polymer
E = activation energy in rate constants, cal/mole
ε = E/RT_s, nondimensional activation energy
F = $\varepsilon(1 - \Theta)$, inner variable
G = function defined after Eq. (47)
h = specific enthalpy
h_i^0 = enthalpy of formation of species i at T_∞
H = $h/c_{p\infty}T_s$ nondimensional specific enthalpy
ΔH = $H_m - H_p$
K = thermal degradation rate constant, polystyrene, Eq. (10)
K' = thermal degradation rate constant, teflon, Eq. (3)
k_i = rate constant for initiation at chain ends, PMMA, Eq. (1)
k_{sc} = random scission rate constant, polystyrene, Eq. (11)
k_w = weak links scission rate constant, polystyrene, Eq. (15)
l = d/r, width of the conduction region
M_m = monomer molar mass
m = mass of sample in isothermal bulk degradation
m_0 = initial mass of sample in isothermal bulk degradation
N_w = number of weak links per monomer unit, polystyrene, Eq. (18)
n = order of the degradation reaction, Eq. (26)
P = degree of polymerization
P_0 = initial degree of polymerization
P_c = critical chain length, at or below which the chain evaporates rather than being further degraded
P_k = kinetic chain length
q = $1/P$
q_0 = $1/P_0$
q = $q\kappa_p/(q_0 + N_w)$
r = surface linear regression rate, cm/sec
$\mathcal{R}^2$ = nondimensional regression rate, Eq. (27)
R^0 = universal gas constant
T = temperature, °K
t = time
V_i = velocity of species i with respect to that of nondegraded polymer
v_i = V_i/r
y = physical coordinate, normal to regressing surface, >0 into gas phase
Y = y/l
α = E_{ps}/E_{sc}
β = B_{ps}/B_{sc}
γ = E_{ps}/E_w
δ = B_{ps}/B_w
κ_i = $\rho_i/\rho_{p\infty}$
Γ = $\Sigma_i\kappa_i(c_i/c_{p\infty})(1 + v_i)$
λ = coefficient of thermal conductivity
Λ = $\lambda/\lambda_{p\infty}$
η = $Y\varepsilon$, inner coordinate
$\dot{\omega}_i$ = rate of production of species i, g/sec cm^3
Ω_i = $\omega_i d/r^2\rho_{p\infty}$
ρ = density
Θ = T/T_s

Subscripts

i = any species present in the sample
m = monomer

Received July 2, 1969; revision received February 9, 1970. This research was supported by the Advanced Research Projects Agency of the Department of Defense and was monitored by the U.S. Army Research Office-Durham under Contract DA-31-124-ARO-D-257. The author wishes to acknowledge encouragement from F. A. Williams. The numerical calculations were performed at the University of California, San Diego, Computer Center.

* Graduate Student and Research Assistant, Department of the Aerospace and Mechanical Engineering Sciences; present address Centre National de Recherches Scientifiques, Paris, France.